PCCP

ROYAL SOCIETY OF CHEMISTRY

PAPER

View Article Online
View Journal | View Issue

Cite this: *Phys. Chem. Chem. Phys.*, 2023, **25**, 23187

The simplest Criegee intermediate CH_2OO reaction with dimethylamine and trimethylamine: kinetics and atmospheric implications†

Yang Chen,‡[abc] Licheng Zhong,‡[cd] Siyue Liu,[ce] Haotian Jiang,[cf] Jiayu Shi,[cg] Yuqi Jin,[bc] Xueming Yang [ch] and Wenrui Dong *[ci]

Received 24th June 2023,
Accepted 8th August 2023

DOI: 10.1039/d3cp02948d

rsc.li/pccp

We have used the OH laser-induced fluorescence (LIF) method to measure the kinetics of the simplest Criegee intermediate (CH_2OO) reacting with two abundant amines in the atmosphere: dimethylamine ($(CH_3)_2NH$) and trimethylamine ($(CH_3)_3N$). Our experiments were conducted under pseudo-first-order approximation conditions. The rate coefficients we report are $(2.15 \pm 0.28) \times 10^{-11}$ cm^3 molecule^{-1} s^{-1} for $(CH_3)_2NH$ at 298 K and 10 Torr, and $(1.56 \pm 0.23) \times 10^{-12}$ cm^3 molecule^{-1} s^{-1} for $(CH_3)_3N$ at 298 K and 25 Torr with Ar as the bath gas. Both reactions exhibit a negative temperature dependence. The activation energy and pre-exponential factors derived from the Arrhenius equation were (-2.03 ± 0.26) kcal mol^{-1} and $(6.89 \pm 0.90) \times 10^{-13}$ cm^3 molecule^{-1} s^{-1} for $(CH_3)_2NH$, and (-1.60 ± 0.24) kcal mol^{-1} and $(1.06 \pm 0.16) \times 10^{-13}$ cm^3 molecule^{-1} s^{-1} for $(CH_3)_3N$. We propose that the electronegativity of the atom in the co-reactant attached to the C atom of CH_2OO, in addition to the dissociation energy of the fragile covalent bonds with H atoms (H–X bond), plays an important role in the 1,2-insertion reactions. Under certain circumstances, the title reactions can contribute to the sink of amines and Criegee intermediates and to the formation of secondary organic aerosol (SOA).

1. Introduction

Carbonyl oxides, known as Criegee intermediates (CIs), play an indispensable role in atmospheric chemistry. In nature, they are formed by the cycloaddition of ozone over the C=C double bond of alkenes,[1] which is highly exothermic (about 48–60 kcal mol^{-1}).[2] The concentration of CIs is therefore directly related to the emission of alkenes into the atmosphere from both natural and anthropogenic sources. It can vary by several orders of magnitude in different regions, and its steady-state concentrations range from 10^3 to 10^6 molecules cm^{-3}.[3,4]

Upon formation, some CIs may be vibrationally excited due to their high exothermicity,[2] termed CIs*. CIs* subsequently undergo several different fates, namely isomerization; decomposition to species such as OH, HO_2, and other radicals; thermalization by collision with the bath gas to form stabilized CIs denoted as SCIs.[5] The unimolecular reactions of SCIs are closely correlated with their own molecular spatial structures.[4,6] SCIs with α-H toward the terminal O atom of the C=O–O group (*syn*-conformer) would undergo α-H transfer to form an intermediate that dissociates to OH.[4] For example, *syn*-CH_3CHOO decomposes to OH from the 1,4-H transfer mechanism *via* vinyl hydrogen peroxide (VHP) at a rate in the range of 124–182 s^{-1}.[7–9] In comparison, *anti*-CH_3CHOO would isomerize to methyl dioxirane from the 1,3-ring closure mechanism at a calculated rate in the range of 53–67.2 s^{-1}.[4,10,11] CH_2OO would isomerize to dioxirane as *anti*-CH_3CHOO to methyl dioxirane.[4] If the dioxirane formed has a high enough internal energy to overcome an energy barrier of about 43 kcal mol^{-1}, it can decompose to small molecules and

[a] *Key Laboratory of Chemical Lasers, Dalian Institute of Chemical Physics, Chinese Academy of Sciences, Dalian, 116023, China*
[b] *University of Chinese Academy of Sciences, Beijing, 100049, China*
[c] *State Key Laboratory of Molecular Reaction Dynamics, Dalian Institute of Chemical Physics, Chinese Academy of Sciences, Dalian, 116023, China. E-mail: wrdong@dicp.ac.cn*
[d] *College of Chemical Engineering, Shenyang University of Chemical Technology, Shenyang, 110142, China*
[e] *Key Laboratory of Materials Modification by Laser, Ion, and Electron Beams, Chinese Ministry of Education, School of Physics, Dalian University of Technology, Dalian, 116024, China*
[f] *Department of Chemical Physics, School of Chemistry and Materials Science, University of Science and Technology of China, Hefei, 230026, China*
[g] *Department of Physics, Dalian Maritime University, Dalian, 116026, Liaoning, China*
[h] *Department of Chemistry, Southern University of Science and Technology, Shenzhen, 518055, China*
[i] *Hefei National Laboratory, Hefei, 230088, China*

† Electronic supplementary information (ESI) available: Experimental conditions, error analysis, fitting parameters, BDE *vs.* rate coefficients for different 1,2-insertion reactions, Troe's fit and calculation of gas-collision limit rate coefficients. See DOI: https://doi.org/10.1039/d3cp02948d

‡ These authors contributed equally to this work.

free radicals, including OH.[12] The rate of OH production from CH_2OO at room temperature has been reported to be in the range of 0.001–0.26 s^{-1}.[13–15] In short, the above OH-producing pathways could be an important source of atmospheric OH radicals, especially under cold and/or dark conditions.[16–18]

The bimolecular reactions of SCIs have been studied extensively because of their potential impact on the atmosphere,[6] an example being the reaction of CH_2OO with SO_2, which has a rate coefficient of $(3.9 \pm 0.7) \times 10^{-11}$ cm^3 $molecule^{-1}$ s^{-1} at 298 K.[19] This reaction produces SO_3, a significant contributor to atmospheric acid rain, as observed by time-resolved step-scan infrared spectroscopy[20] and multiplexed photoionization mass spectrometry (MPIMS).[21] In addition, SCIs were found to react rapidly with various carboxylic acids, with rate coefficients in the order of 10^{-10} cm^3 $molecule^{-1}$ s^{-1}.[22] The typical products were adducts with high molecular weight and low saturated vapor pressure, and were therefore thought to be the major contributors to SOA formation.[22] Furthermore, the reactions of SCIs with H_2O were found to be conformer-dependent,[21] *e.g.*, the rate coefficient of *anti*-CH_3CHOO reacting with H_2O was measured to be $(1.31 \pm 0.26) \times 10^{-14}$ cm^3 $molecule^{-1}$ s^{-1} at 298 K and 4 Torr,[23] while an upper limit of 4×10^{-15} cm^3 $molecule^{-1}$ s^{-1} was estimated for *syn*-CH_3CHOO.[21] The reaction of CH_2OO with H_2O is quite slow, but that with the water dimer is fast, with measured rate coefficients at 298 K of $(3.2 \pm 1.2) \times 10^{-16}$ and $(7.4 \pm 0.6) \times 10^{-12}$ cm^3 $molecule^{-1}$ s^{-1}, respectively.[13,24] However, the reaction with H_2O is one of the most important sinks for atmospheric SCIs because of the much higher concentration of water vapor than other trace gases.[25–28]

Amines, dominated by low molecular weight aliphatic amines with one to six carbon atoms, are important atmospheric organic compounds.[29] There have been a few studies on the reactions of SCIs with amines. Chhantyal-Pun *et al.* measured the rate coefficient of the CH_2OO reaction with CH_3NH_2, and the value from MPIMS was $(4.3 \pm 0.5) \times 10^{-12}$ cm^3 $molecule^{-1}$ s^{-1} at 298 K and 4 Torr (He as buffer gas), and from cavity ring-down spectroscopy (CRDS) was $(4.41 \pm 0.7) \times 10^{-12}$ cm^3 $molecule^{-1}$ s^{-1} at 298 K and 10 Torr (N_2 as buffer gas),[30] respectively. Our group has reported that the high-pressure limit rate coefficient of the CH_2OO reaction with $(CH_3)_3CNH_2$ at 298 K is $(4.95 \pm 0.64) \times 10^{-12}$ cm^3 $molecule^{-1}$ s^{-1}.[31] In addition, compared with the CH_2OO reaction with CH_3NH_2, the electron-induced effect dominates over the steric hindrance effect on the reactivity of the CH_2OO reactions with amines.[31] A study combining MPIMS with high-level theoretical calculations showed that the CH_3CHOO reaction with $(CH_3)_2NH$ proceeds *via* the 1,2-insertion mechanism to produce an amine-functionalized hydroperoxide.[32] A strong dependence of the rate coefficient on the CH_3CHOO conformer was observed, *e.g.*, *anti*-CH_3CHOO reacts with $(CH_3)_2NH$ about 34 000 times faster than *syn*-CH_3CHOO. A similar trend was observed for the *anti*-CH_3CHOO and *syn*-CH_3CHOO reactions with H_2O.[33]

$(CH_3)_2NH$ and $(CH_3)_3N$ are prevalent in the atmosphere, with $(CH_3)_3N$ being the most abundant atmospheric amine in terms of global emissions.[34] Animal husbandry, biomass burning and marine are the major sources of amines, and the estimated global emissions from these three sources are (13 ± 8), (20 ± 11), and 0 Gg N y^{-1} for $(CH_3)_2NH$, and (108 ± 29), (11 ± 4), and 50 Gg N y^{-1} for $(CH_3)_3N$, which are significantly higher than most other types of amines.[34]

In this study, we measured the rate coefficients of CH_2OO reacting with $(CH_3)_2NH$ and $(CH_3)_3N$ at various temperatures and pressures using the OH LIF method. The reaction mechanism was proposed by combining the present results with previous research. The atmospheric implications of the title reactions, especially their contributions to the formation of SOA, are discussed.

2. Experimental section

The experimental apparatus for LIF has been described in detail in our previous work[27,35,36] and only a brief introduction will be given here. The reactions take place in a 75 cm long quartz tube equipped with a capacitance manometer (MKS Baratron) and an exhaust throttle valve (MKS, 653B) to actively control the pressure. The reaction temperature was controlled using a water circulator (Yin Der BL-730) and monitored using a K-type thermocouple.

Liquid CH_2I_2 (Alfa Aeser, >99%) in a glass bubbler was maintained at 35 °C using a water bath and carried into the reaction tube by Ar. A series of calibrated mass flow controllers (MKS, GM50A series) were used to control the flow rate of the gases used, including the buffer gas Ar (99.999%), O_2 (99.995%), $(CH_3)_2NH$ (0.1% seeded in Ar) and $(CH_3)_3N$ (0.5% seeded in Ar). The concentration of CH_2I_2 was measured by the UV absorption method using a deep UV LED (DUV325-H46, Roithner Lasertechnik, center wavelength at 322.4 nm with an FWHM of 11 nm) in combination with an amplified photodetector (PDB450A, Thorlabs). The typical $[CH_2I_2]$ used was approximately 1.5×10^{14} molecules cm^{-3}.

To minimize absorption at the photolysis wavelength by the co-reactants $(CH_3)_2NH$/$(CH_3)_3N$, the fourth/third harmonic of a Nd: YAG laser (266/355 nm) was used to photolyze CH_2I_2. Typical laser fluences were 17 and 90 mJ cm^{-2}. The 282 nm probe laser (2 mm diameter, 40 nJ), corresponding to the $P_1(1)$ line of the (1,0) band of the OH ($A^2\sum^+ (v' = 1) \leftarrow X^2\prod (v'' = 0)$) transition, was generated by frequency doubling a dye laser (Rhodamine 590 dye) pumped by the second harmonic of another high repetition rate Nd: YAG laser (Edgewave INNOSLAB: IS12II-ET, 10 kHz). The time delay between the photolysis and the probe laser was controlled by a digital delay generator (Stanford Research System, DG645). The two laser beams intersected at a right angle in the flow tube, and OH fluorescence generated from the unimolecular decomposition of CH_2OO was detected in the direction perpendicular to the two laser beams. The OH fluorescence of 308 nm (transition of $X^2\prod (v' = 0) \leftarrow A^2\sum^+ (v'' = 0)$) was passed through a quartz lens and a stack of filters (Schott UG11, Semrock FF02-320/40-25 and Semrock FF01-315/15-25) before being amplified by a photomultiplier tube (PMT, Electron PDM9111-CP-TTL). The signals from the PMT were fed to a multichannel scaler (Ortec, MCS-PCI) and recorded on a computer.

To increase the signal-to-noise ratio for data analysis, the signals from 1500 photolysis laser pulses were accumulated for a decay profile.

To assess the linearity of the LIF signal in our experimental setup, we initially measured the rate coefficient for the reaction between CH_2OO and SO_2.[27] This measurement was conducted at 10 Torr and 298 K, using Ar as the bath gas. The derived rate coefficient was $(3.88 \pm 0.13) \times 10^{-11}$ cm^3 molecule^{-1} s^{-1}, which closely aligns with the previous findings of $(3.93 \pm 0.13) \times 10^{-11}$ cm^3 molecule^{-1} s^{-1} obtained using CRDS[37] and $(3.9 \pm 0.7) \times 10^{-11}$ cm^3 molecule^{-1} s^{-1} using MPIMS.[19]

3. Results and discussion

3.1 OH Decay profiles and fitting model

About 3% of CH_2I_2 was photolyzed (see the ESI† for calculation details). The formed CH_2I reacted with O_2 to produce CH_2OO with a branching ratio of about 0.79 at 10 Torr.[38] Thus, the initial concentration of CH_2OO was approximately 4.5×10^{12} cm^{-3}. The formation of CH_2OO was on the time scale of tens of microseconds ([O_2] was approximately 1.5×10^{16} cm^{-3} and $k_{CH_2I+O_2} = 1.50 \times 10^{-12}$ cm^3 molecule^{-1} s^{-1}),[38] much faster than the consumption of CH_2OO, which takes several milliseconds, as shown in Fig. 1. Therefore, the formation of CH_2OO was not included in the kinetics model.

The unimolecular loss of CH_2OO includes:

$$CH_2OO \rightarrow OH + HCO \; k_{1a} \quad \text{(R1a)}$$

$$\rightarrow \text{other products } k_{1b} \quad \text{(R1b)}$$

$$\rightarrow \text{physical losses } k_{1c} \quad \text{(R1c)}$$

(R1c) is dominated by the wall loss.

The OH radicals formed from (R1a) are consumed by species X in the reactor, including IO, CH_2I_2, and amines.

$$OH + X \rightarrow \text{products } k_2 \quad \text{(R2)}$$

OH ($v'' = 0$) together with a small amount of OH ($v'' = 1$) was observed from the unimolecular decomposition of CH_2OO.[14,39,40] In the current experiment, the first probe laser pulse was fired approximately 80 μs after the photolysis laser pulse to allow sufficient relaxation of OH ($v'' \geq 2$) to OH ($v'' = 1$), if present. In our previous study, the rate coefficients derived from fitting the time-dependent profiles of OH ($v'' = 0$) with and without including the relaxation of OH ($v'' = 1$) to OH ($v'' = 0$) in the kinetics model differed by less than 4% at 10 Torr and less than 1% at 50 Torr.[39] Therefore, we do not include OH ($v'' = 1$) in the current kinetics model. The resulting error was included in the error analysis as shown in the ESI.†

Bimolecular reactions of CH_2OO include:

$$CH_2OO + CH_2OO \rightarrow \text{products } k_3 \quad \text{(R3)}$$

$$CH_2OO + (CH_3)_2NH \rightarrow \text{products } k_4 \quad \text{(R4)}$$

$$CH_2OO + (CH_3)_3N \rightarrow \text{products } k_5 \quad \text{(R5)}$$

$$CH_2OO + Y \rightarrow \text{products } k_6 \quad \text{(R6)}$$

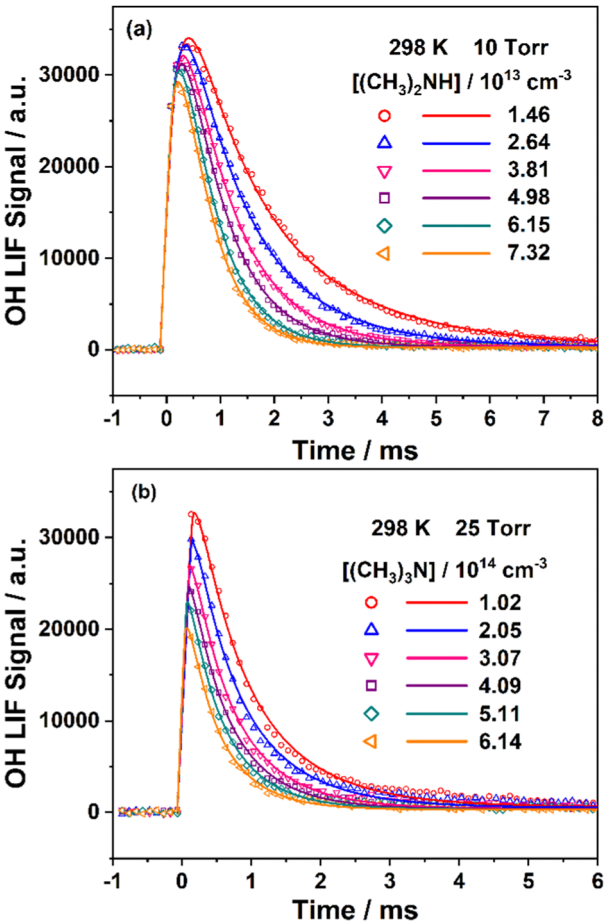

Fig. 1 Representative time-dependent OH profiles in the presence of different concentrations of $(CH_3)_2NH$ (Fig. 1a) and $(CH_3)_3N$ (Fig. 1b) at 298 K. The hollow symbols are the experimental results, and the solid lines are the fits to the experimental results with eqn (1). Time zero was defined by the photolysis laser pulse.

where Y represents species other than CH_2OO or $(CH_3)_2NH$/$(CH_3)_3N$ which consume CH_2OO, including I, IO and CH_2I_2. The concentrations of $(CH_3)_2NH$ and $(CH_3)_3N$ are typically 1–2 orders of magnitude higher than that of CH_2OO to ensure the pseudo-first order approximation conditions for the title reactions. According to previous theoretical calculations, the product of the reaction (R4) would be the insertion product.[32,41]

Applying the pseudo-first order approximation to the reaction (R4) and the steady-state approximation to the OH radicals, the time-dependent signal of OH ($v'' = 0$, $N'' = 1$), $S_{OH}(t)$, can be described by eqn (1) (see our previous work for more details).[27,35,36,42]

$$S_{OH}(t) = \frac{A_0\left(k_1 + k_4' + k_6'\right)}{\left(k_1 + k_4' + k_6'\right)e^{\left(k_1+k_4'+k_6'\right)t} + 2k_3[CH_2OO]_0\left[e^{\left(k_1+k_4'+k_6'\right)t} - 1\right]} - A_1 e^{-k_2' t} \quad (1)$$

where

$$A_0 = \gamma \frac{k_{1a}[CH_2OO]_0}{k_2' - (k_1 + k_4' + k_6')} \quad (2)$$

$$A_1 = \gamma \left(\frac{k_{1a}[CH_2OO]_0}{k_2' - (k_1 + k_4' + k_6')} - [OH]_0 \right) \quad (3)$$

In eqn (1), $k_4' = k_4[(CH_3)_2NH]$, $k_2' = k_2[X]$ and $k_6' = k_6[Y]$. $[CH_2OO]_0$ were calculated from the concentration of CH_2I_2, the photolysis cross section of CH_2I_2 and the pressure-dependent yield of CH_2OO. $[OH]_0$ represents the initial concentration of OH ($v'' = 0$, $N'' = 1$) resulting from $CH_2I^* + O_2$ and/or CH_2OO^*.[14,43] γ is the detection efficiency of OH fluorescence. When fitting the OH decay profiles, A_0, A_1, $k_1 + k_4' + k_6'$ and k_2' are local parameters, while k_3 is a global parameter fixed at 8×10^{-11} cm^3 molecule^{-1} s^{-1} according to the result of Stone *et al.*[44] Reactions (R1) and (R6) are irrelevant to the concentration of $(CH_3)_2NH$. When $k_1 + k_4' + k_6'$ is plotted against $[(CH_3)_2NH]$, the slope and intercept from the linear fit represent k_4 and $k_1 + k_6'$, respectively. Therefore, k_4' can be extracted by subtracting the fitted intercept from $k_1 + k_4' + k_6'$.

Fig. 1 shows the typical time-dependent profiles of OH ($v'' = 0$, $N'' = 1$) from the CH_2OO reactions with $(CH_3)_2NH$ (Fig. 1a, at 10 Torr and 298 K) and $(CH_3)_3N$ (Fig. 1b, at 25 Torr and 298 K). The hollow symbols are experimental data fitted with eqn (1) using the first optimization software (1stOpt 7.0, 7D-soft High Technology Inc.), as shown by solid lines. The OH signals decay faster with increasing concentration of $(CH_3)_2N$ and $(CH_3)_3N$, indicating the consumption of CH_2OO by $(CH_3)_2NH$ and $(CH_3)_3N$.

3.2 Pressure- and temperature-dependent rate coefficients

We first measured the rate coefficients of the title reactions at various pressures and 298 K to determine their high-pressure limits. Fig. 2(a) shows the plot of k_4' against $[(CH_3)_2NH]$ at pressures ranging from 5 to 100 Torr, while Fig. 2(b) displays the plot of k_5' under the same conditions. However, it should be noted that the OH fluorescence signals were quenched more rapidly for reaction (R5), which limited our measurements to pressures above 50 Torr. The rate coefficients for the title reactions at different pressures and 298 K are summarized in Tables S1 and S2 in the ESI.†

Fig. 3 shows the rate coefficients of CH_2OO reacting with $(CH_3)_2NH$ at different pressures from 5 to 100 Torr. No obvious pressure dependence was observed. Although the values at 5 Torr are smaller than those at higher pressures, the difference is within the error bar of the current experiment. A similar non-pressure dependence has been reported for the CH_2OO reactions with NH_3 and CH_3NH_2.[30] Therefore, we believe that the reaction between CH_2OO and $(CH_3)_2NH$ reaches the high-pressure limit at 10 Torr.

In contrast, the pressure dependence of the CH_2OO reaction with $(CH_3)_3N$ is evident, as shown in Fig. 4. Such a pressure

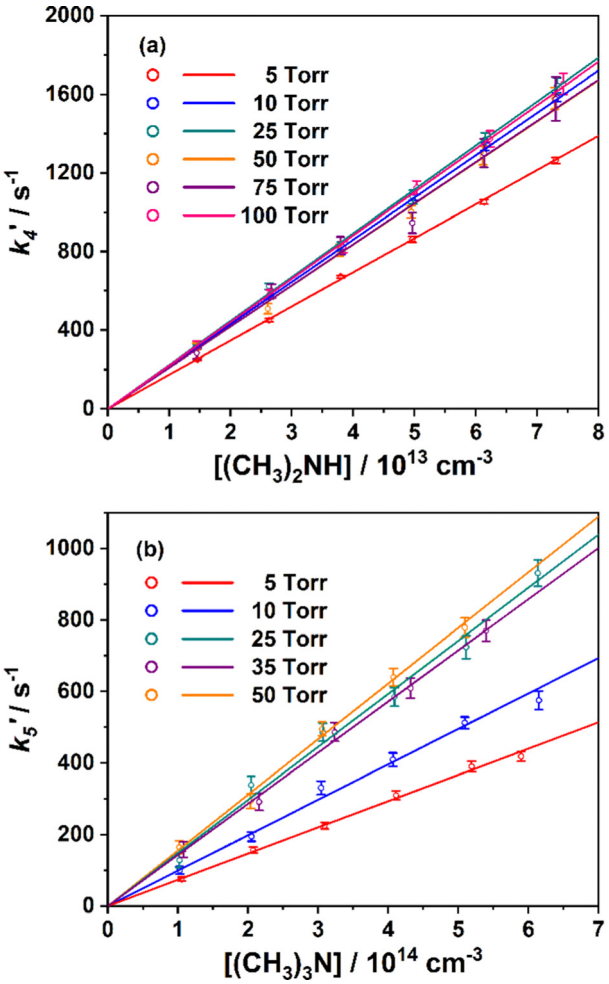

Fig. 2 Plots of the effective loss rate k_4' *versus* $[(CH_3)_2NH]$ (Fig. 2a) and k_5' *versus* $[(CH_3)_3N]$ (Fig. 2b) at different pressures and 298 K. Hollow points are experimental data. Solid lines are linear fits to the experimental data. Error bars of k_4' and k_5' are 1σ uncertainty from the fit of the OH time-dependent profile.

dependence indicates the existence of a submerged barrier between the pre-reactive complex and the reaction product, similar to the 1,2-insertion reaction of *anti*-CH_3CHOO with CH_3OH[45] and cycloaddition reactions of SCIs, *e.g.*, CH_2OO + CH_3CH_2CHO and CH_3COCH_3,[39,46] and $(CH_3)_2COO + SO_2$.[47]

We used a kinetic model based on the Lindemann mechanism to describe the pressure dependence of the CH_2OO reaction with $(CH_3)_3N$. M is the bath gas, and the asterisk indicates high internal energy.

$$CH_2OO + (CH_3)_3N \rightleftharpoons complex^* \quad k_7/k_{-7} \quad (R7)$$

$$Complex^* + M \rightarrow complex + M^* \quad k_8 \quad (R8)$$

$$Complex^* \rightarrow products \quad k_9 \quad (R9)$$

Eqn (4) was used to fit the pressure-dependent rate coefficients, and the result is shown as a red line in Fig. 4, where $[M]$ was derived from the ideal gas equation. From the fit, we

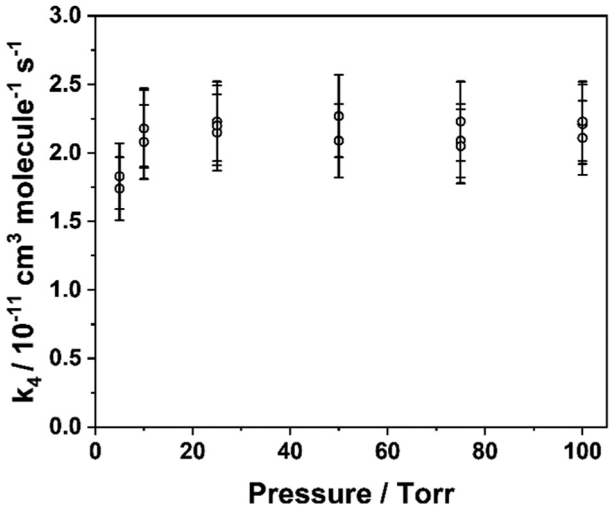

Fig. 3 Rate coefficients of CH_2OO reacting with $(CH_3)_2NH$ as a function of pressure.

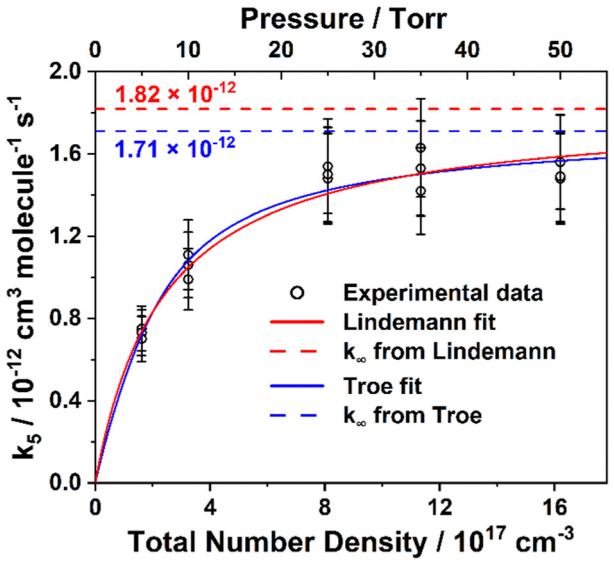

Fig. 4 Rate coefficients of CH_2OO reacting with $(CH_3)_3N$ as a function of the total number density of the bath gas ([M]) at 298 K. The red and blue lines are fitted by the Lindemann mechanism and Troe's treatment, respectively.

obtained a high-pressure limit rate coefficient of 1.82×10^{-12} cm^3 molecule^{-1} s^{-1}.

$$k_5(M) = \frac{k_7[M]}{k_{-7}/k_8 + [M]} \quad (4)$$

Alternatively, we used Troe's treatment, a method for determining the rate coefficients at the high and low pressure limits based on statistical rate theory, to describe the pressure-dependent rate coefficients.[15,48,49] The fitting equation is:

$$k_5 = \left(\frac{k_0[M]}{1 + \frac{k_0[M]}{k_\infty}}\right) \times F_{cent}^{P} \quad (5)$$

where

$$P = \left(1 + \left(\frac{\log_{10}\frac{k_0[M]}{k_\infty}}{N}\right)^2\right)^{-1} \quad (6)$$

$$N = 0.75 - 1.27\log_{10}(F_{cent}) \quad (7)$$

where k_0 and k_∞ are the rate coefficients at the low and high-pressure limits, F_{cent} is the broadening factor, and N is the width parameter. During fitting, the value of F_{cent} was varied between 1.1 and 1.5. When it was set to 1.2, the fit yielded the largest R-square (see Fig. S1 in the ESI†). The resulting fit is represented by a blue line in Fig. 4. By employing Troe's treatment, the high-pressure limit rate coefficient was determined to be 1.71×10^{-12} cm^3 molecule^{-1} s^{-1}, which is in closer agreement with our experimental results compared to the value obtained from the Lindemann mechanism.

The consumption rates of CH_2OO *vs.* $[(CH_3)_2NH]$ (10 Torr) and CH_2OO *vs.* $[(CH_3)_3N]$ (25 Torr) at temperatures from 283 to 318 K are plotted in Fig. 5(a) and (b). The lines are linear fits to the experimental data (hollow symbols). The error bars of k_4' and k_5' represent the 1σ uncertainty of the fit to the time-dependent OH ($v'' = 0$) decay profiles with eqn (1). The larger error bar of k_5' is attributed to the higher pressure used, which resulted in increased collisional quenching of the OH signals and led to a larger uncertainty. The negative temperature dependence of the title reactions, as evidenced by the steeper slope at lower temperatures, suggests the presence of a submerged barrier. After averaging the results of five sets of experimental data at the same temperature (see Tables S4 and S5 for details, ESI†), we report the rate coefficients of CH_2OO reacting with $(CH_3)_2NH$ as (2.55 ± 0.33), (2.15 ± 0.28), (1.92 ± 0.25), and $(1.71 \pm 0.22) \times 10^{-11}$ cm^3 molecule^{-1} s^{-1} at 283, 298, 308 and 318 K, respectively. The rate coefficients for CH_2OO reacting with $(CH_3)_3N$ are (1.82 ± 0.27), (1.56 ± 0.23), (1.44 ± 0.22), and $(1.33 \pm 0.20) \times 10^{-12}$ cm^3 molecule^{-1} s^{-1} at the same temperatures.

The Arrhenius plots for the title reactions are shown in Fig. 6. The experimental data are represented by hollow circles, while the blue and red lines indicate the fits to k_4 and k_5 using the following Arrhenius equation: $k(T) = A\exp(-E_a/RT)$. The error bar represents the total experimental error, estimated to be 13% for $(CH_3)_2NH$ and 15% for $(CH_3)_3N$ (see the ESI†). The activation energy of (-2.03 ± 0.26) kcal mol^{-1} and the pre-exponential factor of $(6.89 \pm 0.90) \times 10^{-13}$ cm^3 molecule^{-1} s^{-1} were derived for CH_2OO reacting with $(CH_3)_2NH$, while (-1.60 ± 0.24) kcal mol^{-1} and $(1.06 \pm 0.16) \times 10^{-13}$ cm^3 molecule^{-1} s^{-1} were determined for CH_2OO reacting with $(CH_3)_3N$.

Alternatively, the temperature-dependent rate coefficients can be described using statistical thermodynamics and transition state (TS) theory.[30] The reaction rate can be written as follows:

$$k(T) = AT^2\exp\left(-\frac{\Delta H}{RT}\right) \quad (8)$$

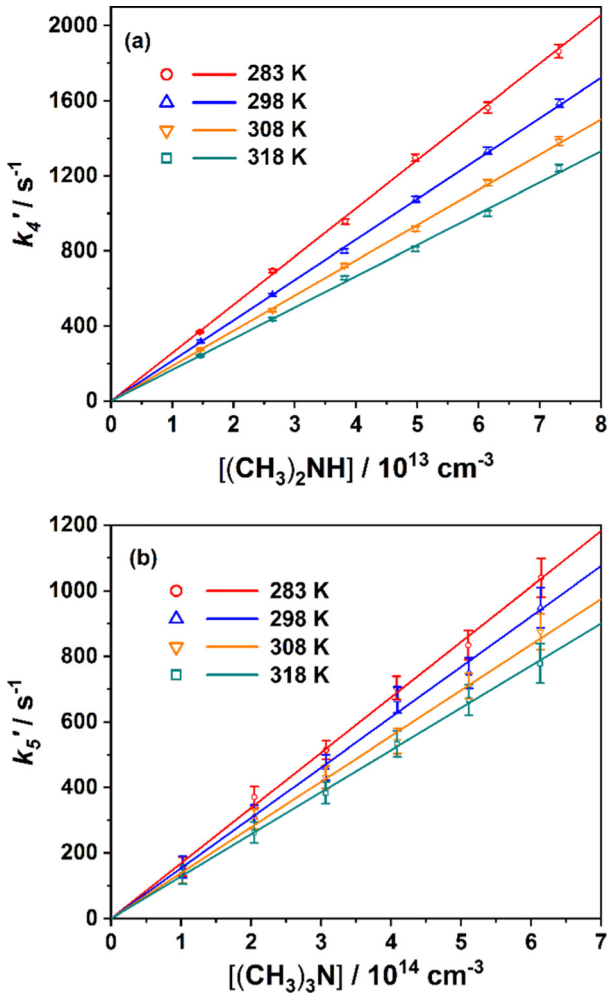

Fig. 5 The effective loss rates k_4' and k_5' plotted against the concentrations of $(CH_3)_2NH$ at 10 Torr (Fig. 5a) and $(CH_3)_3N$ at 25 Torr (Fig. 5b) at four different temperatures. The error bar represents the 1σ uncertainty of the fit to the time-dependent OH ($v'' = 0$) decay profiles with eqn (1).

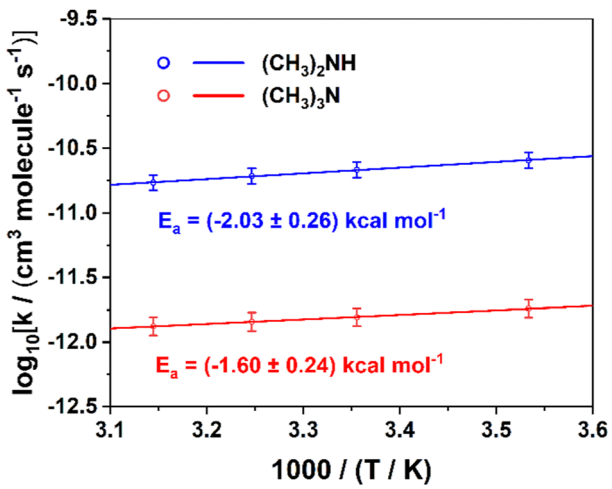

Fig. 6 The Arrhenius plots of the rate coefficients at four different temperatures for the title reactions. The error bars are 13% and 15% of the corresponding rate coefficients.

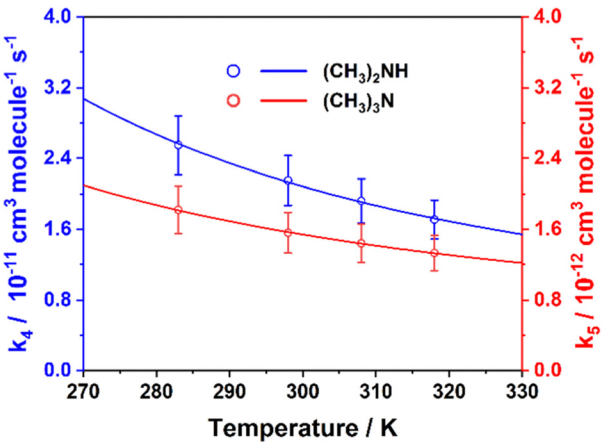

Fig. 7 The rate coefficients k_4 and k_5 at different temperatures were fitted with eqn (8).

where

$$A = \frac{R' k_B}{N_A h} \exp\left(\frac{\Delta S}{R}\right) \quad (9)$$

In the above equations, ΔH and ΔS are the enthalpy and entropy changes. R' and R are molar gas constants expressed in different units, which are 82.1 cm^3 atm mol^{-1} K^{-1} and 8.314 J mol^{-1} K^{-1}, respectively. N_A, k_B and h are the Avogadro, Boltzmann and Planck constants, respectively. The temperature-dependent rate coefficients of the title reactions were fitted with eqn (8) as shown in Fig. 7, and the fit parameters are summarized in Table 1. The enthalpy change of CH_2OO + $(CH_3)_2NH$ (−3.22 kcal mol^{-1}) is more negative than those of the reactions of CH_2OO with NH_3 (−2.01 kcal mol^{-1}) and CH_3NH_2 (−2.75 kcal mol^{-1}).[30] This finding is consistent with the trend that the reaction barrier decreases with increasing methyl substitution on ammonia.[30,41]

3.3 Reaction mechanism

Based on theoretical calculations, Kumar *et al.* proposed that the reaction between CH_2OO and $(CH_3)_2NH$ proceeds by the 1,2-insertion mechanism and is barrierless. They suggested that this reaction should proceed with a rate coefficient similar to the barrierless reactions of CH_2OO with HNO_3 and HCOOH, with rate coefficients in the order of 10^{-10} cm^3 molecule^{-1} s^{-1}.[41] However, our findings indicate that the rate coefficient of the CH_2OO reaction with $(CH_3)_2NH$ is comparable to that of the CH_2OO reaction with HCl, which has a low energy barrier of only 0.5 kJ mol^{-1} between the pre-reactive complex and the transition state, as calculated by Cabezas and Endo.[50] We hypothesize that the CH_2OO reaction with $(CH_3)_2NH$ may have a small submerged barrier, which may be challenging to find depending on the accuracy of the calculations at different levels.

For most 1,2-insertion reactions of CH_2OO (except reactions with species such as H_2S and CH_3SH), an approximately linear relationship has been proposed between the logarithm of the rate coefficients and the bond dissociation energy (BDE) of the

Table 1 A list of parameters obtained by fitting the temperature-dependent rate coefficients of the title reactions with eqn (8)

Co-reactant	A (cm^3 s^{-1} K^{-2})	ΔS (kcal mol^{-1} K^{-1})	ΔH (kcal mol^{-1})
$(CH_3)_2NH$	$(1.04 \pm 0.12) \times 10^{-18}$	-29.43 ± 0.24	-3.22 ± 0.07
$(CH_3)_3N$	$(1.59 \pm 0.08) \times 10^{-19}$	-33.17 ± 0.10	-2.79 ± 0.03

fragile covalent bonds with H atoms (H–X bond) of the co-reactants,[6] which is illustrated in Fig. 8. The BDE and rate coefficients are summarized in Table S8 (ESI†). Regarding the reaction between CH_2OO and $(CH_3)_3N$, CH_2OO is likely to insert into the C–H bond of methyl due to the absence of an H atom attached to the central N atom. The C–H bond of $(CH_3)_3N$, with a BDE of 351 kJ mol^{-1}, is more fragile than the N–H bond of $(CH_3)_2NH$, which has a BDE of 382.8 kJ mol^{-1}.[51] This is easy to understand since a higher BDE tends to hinder the insertion of Criegee intermediates.

As shown in Fig. 8, the rate coefficient of the CH_2OO reaction with $(CH_3)_3N$ is apparently out of line and an order of magnitude smaller than that of $(CH_3)_2NH$, which contradicts the established rule for 1,2-insertion reactions based on BDE. This suggests that other factors may influence its reactivity. One possible explanation is that the C atom of CH_2OO forms a bond with the C atom of $(CH_3)_3N$ after insertion into the C–H bond of the methyl group. The newly formed C–C bond is less stable than the C–O and C–N bonds in other 1,2-insertion reactions due to the difference in the electronegativity of the atoms involved. This explanation is supported by the slow rate coefficients of CH_2OO with H_2S and CH_3SH, which are $(1.7 \pm 0.2) \times 10^{-13}$ and $(1.01 \pm 0.17) \times 10^{-12}$ cm^3 $molecule^{-1}$ s^{-1} at 298 K, despite their low BDE of 381.6 and 365.3 kJ mol^{-1},[51] respectively. This is due to the less stable C-S bond, where the attractive forces between the S atom (a third-row element) and the C atom of CH_2OO are weaker than those between the O or N atoms (second-row elements) and the C atom of CH_2OO.[6] The rate coefficient of the reaction between CH_2OO and $(CH_3)_2NH$ is slightly lower than that predicted by the linear model. This can be attributed to the steric hindrance caused by $(CH_3)_2NH$, which is similar to the reaction of CH_2OO with $(CH_3)_3CNH_2$.[31]

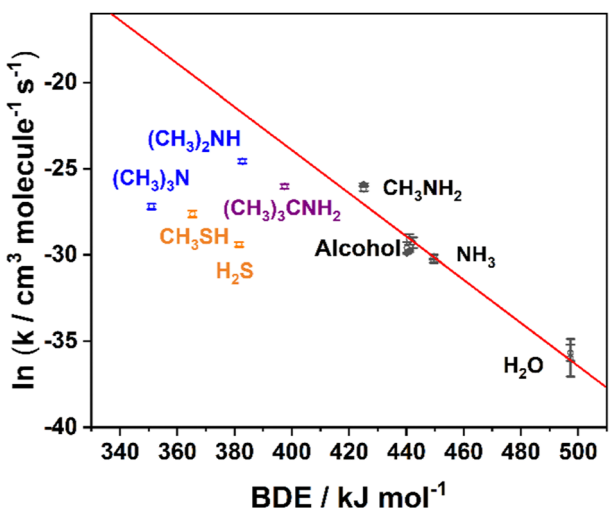

Fig. 8 Comparison of the logarithm of the rate coefficients of several 1,2-insertion reactions of CH_2OO with BDE of the labile hydrogen atom. The red line is a linear fit. The blue points are our experimental results. CH_3OH, C_2H_5OH, and $(CH_3)_2CHOH$ are collectively referred to as alcohol.

4. Atmospheric implications

$(CH_3)_2NH$ and $(CH_3)_3N$ are two types of amines that are abundant in the atmosphere, making their reactions highly representative and informative. One of the primary ways by which amines are removed from the atmosphere is through their reactions with OH radicals.[52] The rate coefficients of OH reacting with $(CH_3)_2NH$ and $(CH_3)_3N$ were measured to be $(6.39 \pm 3.5) \times 10^{-11}$ and $(5.73 \pm 1.5) \times 10^{-11}$ cm^3 $molecule^{-1}$ s^{-1} at 298 K, respectively.[53] The diurnal concentration of OH is approximately 10^6 molecules cm^{-3},[54] while the steady-state peak concentration of all SCIs predicted in the forested equatorial regions by combining field data analysis with a global chemical model is approximately 10^5 molecules cm^{-3}.[4]

A comparison of the atmospheric sink of $(CH_3)_2NH$/$(CH_3)_3N$ by OH and SCIs is shown in Table 2. SCIs cannot compete with OH in the consumption of $(CH_3)_2NH$ and $(CH_3)_3N$, even at the highest concentration of SCIs (10^5 molecules cm^{-3}) used in the calculation. We may also overestimate the contribution of SCIs by assuming that the effective reaction rates of SCIs with $(CH_3)_2NH$ and $(CH_3)_3N$ are the same as that of CH_2OO, as some SCIs react more slowly with amines than CH_2OO, such as the *syn*-CH_3CHOO reaction with $(CH_3)_2NH$.[32] However, during the night and/or cold winter, the concentration of OH radicals decreases due to the lack of UV light and water vapor. For example, at four selected urban sites in the UK, the average steady-state nighttime OH concentration was in the range of 1.8–3.1 $\times$ 10^5 molecules cm^{-3}, and the winter OH concentration in Bristol was about half of its annual maximum.[55] In contrast, the disparity in SCI concentrations between summer and winter was generally less pronounced. For example, the winter concentrations were found to be similar to or approximately two-thirds of the corresponding summer concentration at two urban sites and one rural site in the UK.[56] Under these conditions, SCIs would increase their importance in consuming $(CH_3)_2NH$ and $(CH_3)_3N$. At temperatures in the troposphere, such as 230 K, the rate coefficients of the OH reactions with $(CH_3)_2NH$ and $(CH_3)_3N$ increase by less than 20%, to 7.76×10^{-11} and 6.89×10^{-11} cm^3 $molecule^{-1}$ s^{-1},[53] while those for the reactions with CH_2OO increase more than two-fold, to 5.86×10^{-11} and 3.52×10^{-12} cm^3 $molecule^{-1}$ s^{-1}.

Table 2 Comparison of the consumption of $(CH_3)_2NH$ and $(CH_3)_3N$ by OH and SCIs. τ is the lifetime of the corresponding species, calculated assuming [OH] = 10^6 molecules cm^{-3} and [SCIs] = 10^5 molecules cm^{-3}

Co-reactant	τ_{OH} (days)	τ_{SCIs} (days)	τ_{SCIs}/τ_{OH}
$(CH_3)_2NH$	0.18	5.38	30
$(CH_3)_3N$	0.20	74.19	371

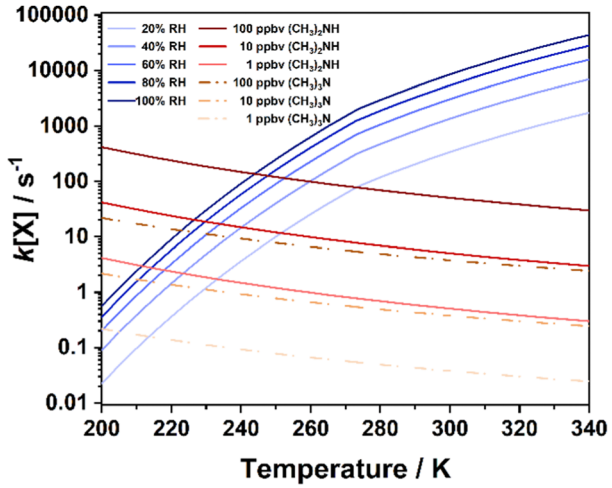

Fig. 9 Comparison of the loss rate of CH_2OO by $(H_2O)_2$ and $(CH_3)_2NH$/$(CH_3)_3N$ in the temperature range of 200–340 K.

This indicates that reactions with CH_2OO are more competitive than those with OH as the temperature decreases.

The primary sinks of SCIs are their unimolecular reactions[7,9,11,28] and some bimolecular reactions, which are dominated by water vapor in the case of CH_2OO.[25,26,28] However, reactions with amines can also be additional sources of SCI consumption in certain regions. Fig. 9 shows the consumption rates of CH_2OO by water vapor (including both the monomer and dimer), $(CH_3)_2NH$ and $(CH_3)_3N$ at various relative humidities and temperatures. The value of $[(H_2O)_2]$ was obtained from the equilibrium constant between H_2O and $(H_2O)_2$, relative humidity, and saturated vapor pressure.[57,58] $[(CH_3)_2NH]$ and $[(CH_3)_3N]$ were varied from 1–100 ppbv, because their maximum concentration was reported to be about 100 ppbv in the industrial area.[59] Fig. 9 indicates that in the upper troposphere, typically below 230 K, $(CH_3)_2NH$ and $(CH_3)_3N$ are comparable to water vapor in the consumption of CH_2OO. In addition, the reaction of CH_2OO with NH_3 can be catalyzed by water vapor,[60] and such reactions are important in the consumption of SCIs in regions where both relative humidity and amines are high.

The title reactions, along with other 1,2-insertion reactions, can produce functionalized organic hydroperoxides with high molecular weight and low saturated vapor pressure. The hydroperoxides have the potential to partition into organic aerosols in the particle phase. It has been shown that multiple CH_2OO can continuously insert into the adduct product of the reaction between a single CH_2OO and amines, resulting in the formation of low-volatility oligomers that make substantial contribution to the formation of SOA.[41]

Amines have been shown to be more efficient than NH_3 in particle formation. For example, experiments conducted in the CLOUD chamber at CERN demonstrated that $(CH_3)_2NH$ above 3 ppt by volume can enhance particle formation rates more than 1000-fold compared to NH_3.[61] Similarly, $(CH_3)_3CNH_2$ was found to be more effective than NH_3 in nucleation from the reaction of OH radicals with SO_2.[62] Various amines have also been found to enhance H_2SO_4 aerosol nucleation more than NH_3.[63] The rate coefficient of the CH_2OO reaction with NH_3 is reported to be about 5.6×10^{-14} cm^3 molecule^{-1} s^{-1}, which is one to two orders smaller than those of the title reactions.[27,35,36,42] Therefore, even though the concentrations of dimethylamine and trimethylamine being approximately two to three orders of magnitude lower than that of NH_3,[34] their contribution to the formation of SOA from the reactions with SCIs is comparable to that of NH_3.

5. Conclusions

Using the LIF method, we measured the rate coefficients of CH_2OO reacting with $(CH_3)_2NH$ and $(CH_3)_3N$. We reported the rate coefficients at 298 K for CH_2OO reacting with $(CH_3)_2NH$ as $(2.15 \pm 0.28) \times 10^{-11}$ cm^3 molecule^{-1} s^{-1}, and with $(CH_3)_3N$ as $(1.56 \pm 0.23) \times 10^{-12}$ cm^3 molecule^{-1} s^{-1} at 10 and 25 Torr using Ar as the bath gas, respectively. The Arrhenius plot yielded an activation energy of (-2.03 ± 0.26) kcal mol^{-1} and a pre-exponential factor of $(6.89 \pm 0.90) \times 10^{-13}$ cm^3 molecule^{-1} s^{-1} for the reaction of CH_2OO with $(CH_3)_2NH$, and (-1.60 ± 0.24) kcal mol^{-1} and $(1.06 \pm 0.16) \times 10^{-13}$ cm^3 molecule^{-1} s^{-1} for the reaction of CH_2OO with $(CH_3)_3N$. The rate coefficients of the title reaction are higher than those of CH_2OO with NH_3 and CH_3NH_2 due to the smaller BDE of $(CH_3)_2NH$ (382.8 kJ mol^{-1}) and $(CH_3)_3N$ (351 kJ mol^{-1}). The rate coefficient of CH_2OO reacting with $(CH_3)_3N$ is about an order of magnitude lower than that of $(CH_3)_2NH$, possibly because the newly formed C–C bond (in the former reaction) is less stable than the C–N bond (in the latter reaction) due to the electronegativity of the atoms involved. In addition, the title reactions can contribute to the consumption of amines and SCIs and the formation of SOA under certain conditions.

Conflicts of interest

The authors declare no competing financial interest.

Acknowledgements

The authors gratefully acknowledge the Dalian Coherent Light Source (DCLS) for support and assistance. This work was funded by the National Natural Science Foundation of China (NSFC No. 22288201), Chinese Academy of Sciences (GJJSTD20220001), and Innovation Program for Quantum Science and Technology (no. 2021ZD0303305).

References

1 R. Criegee, *Angew. Chem. Int. Ed. Engl.*, 1975, **14**, 745–752.
2 D. Johnson and G. Marston, *Chem. Soc. Rev.*, 2008, **37**, 699–716.
3 A. Novelli, K. Hens, C. T. Ernest, M. Martinez, A. C. Nolscher, V. Sinha, P. Paasonen, T. Petaja, M. Sipila, T. Elste, C. Plass-Dulmer, G. J. Phillips, D. Kubistin, J. Williams, L. Vereecken, J. Lelieveld and H. Harder, *Atmos. Chem. Phys.*, 2017, **17**, 7807–7826.

4 L. Vereecken, A. Novelli and D. Taraborrelli, *Phys. Chem. Chem. Phys.*, 2017, **19**, 31599–31612.
5 M. Pfeifle, Y. T. Ma, A. W. Jasper, L. B. Harding, W. L. Hase and S. J. Klippenstein, *J. Chem. Phys.*, 2018, **148**, 174306.
6 R. Chhantyal-Pun, M. A. H. Khan, C. A. Taatjes, C. J. Percival, A. J. Orr-Ewing and D. E. Shallcross, *Int. Rev. Phys. Chem.*, 2020, **39**, 383–422.
7 X. H. Zhou, Y. Q. Liu, W. R. Dong and X. M. Yang, *J. Phys. Chem. Lett.*, 2019, **10**, 4817–4821.
8 T. L. Nguyen, L. McCaslin, M. C. McCarthy and J. F. Stanton, *J. Chem. Phys.*, 2016, **145**, 131102.
9 Y. L. Li, M. T. Kuo and J. M. Lin, *RSC Adv.*, 2020, **10**, 8518–8524.
10 K. T. Kuwata, M. R. Hermes, M. J. Carlson and C. K. Zogg, *J. Phys. Chem. A*, 2010, **114**, 9192–9204.
11 C. Robinson, L. Onel, J. Newman, R. Lade, K. D. Au, L. Sheps, D. E. Heard, P. W. Seakins, M. A. Blitz and D. Stone, *J. Phys. Chem. A*, 2022, **126**, 6984–6994.
12 T. L. Nguyen, H. Lee, D. A. Matthews, M. C. McCarthy and J. F. Stanton, *J. Phys. Chem. A*, 2015, **119**, 5524–5533.
13 T. Berndt, R. Kaethner, J. Voigtlander, F. Stratmann, M. Pfeifle, P. Reichle, M. Sipila, M. Kulmala and M. Olzmann, *Phys. Chem. Chem. Phys.*, 2015, **17**, 19862–19873.
14 D. Stone, K. Au, S. Sime, D. J. Medeiros, M. Blitz, P. W. Seakins, Z. Decker and L. Sheps, *Phys. Chem. Chem. Phys.*, 2018, **20**, 24940–24954.
15 J. Peltola, P. Seal, A. Inkila and A. Eskola, *Phys. Chem. Chem. Phys.*, 2020, **22**, 11797–11808.
16 Y. Lu and M. A. K. Khalil, *Chemosphere*, 1991, **23**, 397–444.
17 F. Holland, A. Hofzumahaus, R. Schafer, A. Kraus and H. W. Patz, *J. Geophys. Res.: Atmos.*, 2003, **108**, PHO 2-1–PHO 2-23.
18 M. A. H. Khan, C. J. Percival, R. L. Caravan, C. A. Taatjes and D. E. Shallcross, *Environ. Sci.-Process Impacts*, 2018, **20**, 437–453.
19 O. Welz, J. D. Savee, D. L. Osborn, S. S. Vasu, C. J. Percival, D. E. Shallcross and C. A. Taatjes, *Science*, 2012, **335**, 204–207.
20 Y. Y. Wang, M. R. Dash, C. Y. Chung and Y. P. Lee, *J. Chem. Phys.*, 2018, **148**, 064301.
21 C. A. Taatjes, O. Welz, A. J. Eskola, J. D. Savee, A. M. Scheer, D. E. Shallcross, B. Rotavera, E. P. F. Lee, J. M. Dyke, D. K. W. Mok, D. L. Osborn and C. J. Percival, *Science*, 2013, **340**, 177–180.
22 R. Chhantyal-Pun, B. Rotavera, M. R. McGillen, M. A. H. Khan, A. J. Eskola, R. L. Caravan, L. Blacker, D. P. Tew, D. L. Osborn, C. J. Percival, C. A. Taatjes, D. E. Shallcross and A. J. Orr-Ewing, *ACS Earth Space Chem.*, 2018, **2**, 833–842.
23 L. C. Lin, W. Chao, C. H. Chang, K. Takahashi and J. J. M. Lin, *Phys. Chem. Chem. Phys.*, 2016, **18**, 28189–28197.
24 M. C. Smith, C. H. Chang, W. Chao, L. C. Lin, K. Takahashi, K. A. Boering and J. J. M. Lin, *J. Phys. Chem. Lett.*, 2015, **6**, 2708–2713.
25 T. R. Lewis, M. A. Blitz, D. E. Heard and P. W. Seakins, *Phys. Chem. Chem. Phys.*, 2015, **17**, 4859–4863.
26 L. C. Lin, H. T. Chang, C. H. Chang, W. Chao, M. C. Smith, C. H. Chang, J. J. M. Lin and K. Takahashi, *Phys. Chem. Chem. Phys.*, 2016, **18**, 4557–4568.
27 Y. Q. Liu, F. H. Liu, S. Y. Liu, D. X. Dai, W. R. Dong and X. M. Yang, *Phys. Chem. Chem. Phys.*, 2017, **19**, 20786–20794.
28 B. Long, J. L. Bao and D. G. Truhlar, *J. Am. Chem. Soc.*, 2016, **138**, 14409–14422.
29 J. H. Seinfeld, *Environ. Sci. Technol.*, 1986, **20**, 863.
30 R. Chhantyal-Pun, R. J. Shannon, D. P. Tew, R. L. Caravan, M. Duchi, C. Wong, A. Ingham, C. Feldman, M. R. McGillen, M. A. H. Khan, I. O. Antonov, B. Rotavera, K. Ramasesha, D. L. Osborn, C. A. Taatjes, C. J. Percival, D. E. Shallcross and A. J. Orr-Ewing, *Phys. Chem. Chem. Phys.*, 2019, **21**, 14042–14052.
31 Y. Chen, H. T. Jiang, S. Y. Liu, J. Y. Shi, Y. Q. Jin, X. M. Yang and W. R. Dong, *J. Phys. Chem. A*, 2023, **127**, 2432–2439.
32 M. F. Vansco, M. J. Zou, I. O. Antonov, K. Ramasesha, B. Rotavera, D. L. Osborn, Y. Georgievskii, C. J. Percival, S. J. Klippenstein, C. A. Taatjes, M. I. Lester and R. L. Caravan, *J. Phys. Chem. A*, 2022, **126**, 710–719.
33 L. C. Lin, H. T. Chang, C. H. Chang, W. Chao and K. Takahashi, *Phys. Chem. Chem. Phys.*, 2016, **18**, 4557.
34 X. L. Ge, A. S. Wexler and S. L. Clegg, *Atmos. Environ.*, 2011, **45**, 524–546.
35 S. Y. Liu, X. H. Zhou, Y. Chen, Y. Q. Liu, S. R. Yu, K. Takahashi, H. B. Ding, Z. F. Ding, X. M. Yang and W. R. Dong, *J. Phys. Chem. A*, 2021, **125**, 8587–8594.
36 X. H. Zhou, Y. Chen, Y. Q. Liu, X. Y. Li, W. R. Dong and X. M. Yang, *Phys. Chem. Chem. Phys.*, 2021, **23**, 13276–13283.
37 R. Chhantyal-Pun, A. Davey, D. E. Shallcross, C. J. Percival and A. J. Orr-Ewing, *Phys. Chem. Chem. Phys.*, 2015, **17**, 3617–3626.
38 W. L. Ting, C. H. Chang, Y. F. Lee, H. Matsui, Y. P. Lee and J. J. M. Lin, *J. Chem. Phys.*, 2014, **141**, 104308.
39 Y. Q. Liu, X. H. Zhou, Y. Chen, M. D. Chen, C. L. Xiao, W. R. Dong and X. M. Yang, *Phys. Chem. Chem. Phys.*, 2020, **22**, 25869–25875.
40 X. H. Zhou, Y. Q. Liu, Y. Chen, X. Y. Li, C. L. Xiao, W. R. Dong and X. M. Yang, *J. Phys. Chem. A*, 2020, **124**, 6125–6132.
41 M. Kumar and J. S. Francisco, *Chem. Sci.*, 2019, **10**, 743–751.
42 Y. Q. Liu, C. T. Yin, M. C. Smith, S. Y. Liu, M. D. Chen, X. H. Zhou, C. L. Xiao, D. X. Dai, J. J. M. Lin, K. Takahashi, W. R. Dong and X. M. Yang, *Phys. Chem. Chem. Phys.*, 2018, **20**, 29669–29676.
43 J. H. Lehman, H. W. Li and M. I. Lester, *Chem. Phys. Lett.*, 2013, **590**, 16–21.
44 Z. S. Mir, T. R. Lewis, L. Onel, M. A. Blitz, P. W. Seakins and D. Stone, *Phys. Chem. Chem. Phys.*, 2020, **22**, 9448–9459.
45 W. Chao, Y.-H. Lin, C. Yin, W.-H. Lin, K. Takahashi and J. J.-M. Lin, *Phys. Chem. Chem. Phys.*, 2019, **21**, 13633–13640.
46 R. Chhantyal-Pun, M. A. H. Khan, R. Martin, N. Zachhuber, Z. J. Buras, C. J. Percival, D. E. Shallcross and A. J. Orr-Ewing, *ACS Earth Space Chem.*, 2019, **3**, 2363–2371.
47 H. L. Huang, W. Chao and J. J. M. Lin, *Proc. Natl. Acad. Sci. U. S. A.*, 2015, **112**, 10857–10862.
48 J. Troe, *Chem. Rev.*, 2003, **103**, 4565–4576.
49 J. Troe, *J. Phys. Chem.*, 1979, **83**, 114–126.

50 C. Cabezas and Y. Endo, *Chem. Phys. Chem.*, 2017, **18**, 1860–1863.
51 W. M. Haynes, *CRC Handbook of Chemistry and Physics*, Crc Press, 2016, vol. 257, p. 423.
52 C. J. Nielsen, H. Herrmann and C. Weller, *Chem. Soc. Rev.*, 2012, **41**, 6684–6704.
53 L. Onel, L. Thonger, M. A. Blitz and P. W. Seakins, *J. Phys. Chem. A*, 2013, **117**, 10736–10745.
54 D. Stone, L. K. Whalley and D. E. Heard, *Chem. Soc. Rev.*, 2012, **41**, 6348–6404.
55 M. A. H. Khan, M. M. N. Hoque, S. S. Alam, M. J. Ashfold, G. Nickless and D. E. Shallcross, *J. Environ. Sci.*, 2011, **23**, 60–64.
56 M. A. H. Khan, W. C. Morris, M. Galloway, B. A. Shallcross, C. J. Percival and D. E. Shallcross, *Int. J. Chem. Kinet.*, 2017, **49**, 611–621.
57 B. Ruscic, *J. Phys. Chem. A*, 2013, **117**, 11940–11953.
58 A. L. Buck, *J. Appl. Meteorol. Climatol.*, 1981, **20**, 1527–1532.
59 S. Fuselli, G. Benedetti and R. Mastrangeli, *Atmos. Environ.*, 1982, **16**, 2943–2946.
60 W. Chao, C. T. Yin, K. Takahashi and J. J. M. Lin, *Phys. Chem. Chem. Phys.*, 2019, **21**, 22589–22597.
61 J. Almeida, S. Schobesberger, A. Kurten, I. K. Ortega, O. Kupiainen-Maatta, A. P. Praplan, A. Adamov, A. Amorim, F. Bianchi, M. Breitenlechner, A. David, J. Dommen, N. M. Donahue, A. Downard, E. Dunne, J. Duplissy, S. Ehrhart, R. C. Flagan, A. Franchin, R. Guida, J. Hakala, A. Hansel, M. Heinritzi, H. Henschel, T. Jokinen, H. Junninen, M. Kajos, J. Kangasluoma, H. Keskinen, A. Kupc, T. Kurten, A. N. Kvashin, A. Laaksonen, K. Lehtipalo, M. Leiminger, J. Leppa, V. Loukonen, V. Makhmutov, S. Mathot, M. J. McGrath, T. Nieminen, T. Olenius, A. Onnela, T. Petaja, F. Riccobono, I. Riipinen, M. Rissanen, L. Rondo, T. Ruuskanen, F. D. Santos, N. Sarnela, S. Schallhart, R. Schnitzhofer, J. H. Seinfeld, M. Simon, M. Sipila, Y. Stozhkov, F. Stratmann, A. Tome, J. Trostl, G. Tsagkogeorgas, P. Vaattovaara, Y. Viisanen, A. Virtanen, A. Vrtala, P. E. Wagner, E. Weingartner, H. Wex, C. Williamson, D. Wimmer, P. L. Ye, T. Yli-Juuti, K. S. Carslaw, M. Kulmala, J. Curtius, U. Baltensperger, D. R. Worsnop, H. Vehkamaki and J. Kirkby, *Nature*, 2013, **502**, 359–363.
62 T. Berndt, F. Stratmann, M. Sipila, J. Vanhanen, T. Petaja, J. Mikkila, A. Gruner, G. Spindler, R. L. Mauldin, J. Curtius, M. Kulmala and J. Heintzenberg, *Atmos. Chem. Phys.*, 2010, **10**, 7101–7116.
63 H. Yu, R. McGraw and S. H. Lee, *Geophys. Res. Lett.*, 2012, **39**, L02807.

